DISCLAIMER

SLAC-PUB-1761
LBL-4890
May 1976
(E/I)

TEST OF A LEAD-LIQUID ARGON ELECTROMAGNETIC SHOWER DETECTOR*

D. Hitlin, J. F. Martin and C. C. Morehouse

Stanford Linear Accelerator Center
Stanford University, Stanford, California 94305

and

G. S. Abrams, D. Briggs, W. Carithers, S. Cooper, R. DeVoe, C. Friedberg, D. Marsh, S. Shannon, E. Vella and J. S. Whitaker.

Lawrence Berkeley Laboratory and Department of Physics
University of California, Berkeley, California 94720

ABSTRACT

The design and construction of two lead-liquid argon electromagnetic shower detectors are described. Test results in beams of electrons and π^- of momenta .125 - 4 GeV/c and 1 - 4 GeV/c respectively are presented. Measurements were made of the energy resolution for electromagnetic showers, the position resolution, the behavior of the device in a transverse magnetic field and the radial and longitudinal characteristics of energy deposition, especially as they apply to π^-/e^- discrimination.

(Submitted to Nuclear Instruments & Methods)

*Work supported by the Energy Research and Development Administration.

1. Introduction

The recent development of liquid argon ionization chambers for hadron calorimeters and electromagnetic shower counters has made it possible to equip large 4π detectors at storage rings with electromagnetic detectors which have both good spatial and energy resolution. We will describe tests of small ionization chambers with thin lead radiators divided into 2 cm. wide strips. The results of these tests have been sufficiently encouraging for us to design a large system of ten modules which will provide the electromagnetic detection capability of the new SPEAR Mark II Detector Facility at SLAC.

The use of liquid argon to sample the ionization produced in a hadronic or electromagnetic cascade was pioneered by Willis. An excellent introduction to these devices is provided in the papers of Willis and Radeka[1], Engler, et al.,[2] and Knies and Neuffer[3]. We will therefore not dwell on details of the theory of the device or the associated electronic circuitry.

2. Design and Construction

A lead/liquid argon device measures the energy of a shower by sampling the total ionization energy loss of the shower products. On the basis of electromagnetic shower theory one would expect the device to be linear[4] if all the shower energy is contained, and the distribution of sampled tracks to be nearly Gaussian with an r.m.s. width (energy resolution) inversely proportional to the square root of the plate thickness ($\sigma \sim t^{-\frac{1}{2}}$). Since there are a large number of very low energy particles in the shower, this approximation will not be valid below a given plate thickness. Monte Carlo studies indeed indicate

that for a sampling device with alternate layers of lead and liquid argon, the resolution at 1 GeV/c does improve as $t^{-\frac{1}{2}}$ in the region down to plate thicknesses of ~.2 r.l., but then improves more quickly for finer sampling (see Figure 1).

In order to test the dependence of resolution on sampling thickness, as well as to try different construction techniques and readout schemes, two modules were constructed. Both used 2 cm. wide readout strips, with all strips oriented in the same direction. The active volume of both modules was 23 cm. x 24.5 cm. x ~30 cm. deep.

In the first detector (henceforth A) a unit cell consisted of a 1.1 mm. Pb sheet, 2 mm. of liquid argon, a 2.3 mm. Pb/G10 laminate with the lead segmented into 2 cm. strips, and 2 mm. of liquid argon. Detector A was constructed of 42 such unit cells for a total depth of 15.75 r.l. Each laminate consisted of 11 lead strips, 2 cm. wide x 0.42 mm. thick, glued (with 3M #3549 Structural Adhesive) to both sides of a 1.2 mm. thick sheet of NEMA G10 fiberglass. (This lamination technique was found to have sufficient shear strength to withstand the differential contraction of at least 3 meters of Pb/G10 sandwich at liquid nitrogen temperature). Ceramic washers maintained the 2 mm. gap spacing. The entire structure was clamped together from the outside corners. The Pb sheets were at ground, and the lead strips were at negative high voltage, the signal being coupled out through 0.01 μf capacitors.

For the second module (henceforth B) the solid planes were 2.2 mm. Pb sheets and the 2 cm. wide readout strips were constructed from etched copper-clad G10 circuit board material. The structure was clamped with

threaded G10 rods and the 2 mm. gap spacing was maintained with ceramic washers. This device consisted of 36 unit cells and was also 15.75 r.l. deep. In this module the solid sheets were connected to high voltage and the signal was taken from the printed circuit strips at ground. Decoupling was accomplished at each solid plate through a 0.01 μf capacitor. The electrical performance of the two modules was essentially identical, but the second scheme of high voltage distribution requires fewer large capacitors.

Sixteen channels of readout electronics were constructed; unit cells in both modules were therefore grouped together as shown in Figure 2. This configuration was chosen to allow the study of longitudinal and radial energy deposition in some detail, especially as they pertained to the spatial resolution and π/e rejection capability of the device. The capacitance of the individual channels varied from 200pf to 2400pf. Signals were carried to a feedthrough with short lengths of RG174 coaxial cable.

The preamplifiers, mounted directly on the dewar, were of a design used by the Willis group at CERN[5], with some minor changes. For ease of winding, Ferroxcube 3D3 pot cores were used for the input transformer in place of the toroidal type used by Willis. The low noise FET used was a selected TIS75. Sixty percent of a sample of 100 of these inexpensive FET's were found to have a noise figure of $\leq$ 1.1 nV/$\sqrt{\text{Hz}}$ at 100 kHz. The preamplifiers drove twisted pair lines to bipolar shaping amplifiers, also of a design used by Willis. With a shaping time of 0.6 μsec, the equivalent noise charge varied from 4,000 r.m.s. electrons for channels with 200pf capacitance to 12,000 r.m.s. electrons for 2400pf

channels. The outputs of the shaping amplifiers were digitized in LeCroy #2249 ADC's, gated for $\pm$ 75 nsec about the peak.

Relative calibration of the gain of each of the sixteen channels was accomplished by applying a long pulse of known amplitude to small (10pf per 200pf of channel capacitance) silver mica capacitors mounted within the dewar close to each strip group. The input pulse was varied over a range of 15 mV ($\sim 10^6$ electrons for a 10pf calibration capacitor) and the ADC output was recorded for each step. The long term stability of the electronics was found to be better than 1%.

The modules were contained in an upright stainless steel dewar 150 cm. deep by 45 cm. inside diameter. The dewar had an entrance port for the beam consisting of 0.5 mm. of stainless steel in two windows and 2 cm. of liquid argon, for a total of 0.1 r.l. The fill cycle began with several cycles of alternately filling with argon gas and evacuating to 50 microns. Argon gas was condensed with a heat exchanger coil filled with liquid nitrogen. The argon used was either "Pre-purified" grade gas or the boiloff from 130 liter dewars of welding grade liquid argon. Approximately 75 liters of liquid were needed to cover the module assembly. Regulation of the argon space pressure (approximately 1 psig) was accomplished by controlling the liquid nitrogen flow through the heat exchanger, which consisted of 5 meters of copper tubing. During the fill and at regular intervals througout the test, the oxygen impurity in the argon gas in equilibrium with the liquid was tested by measuring the burnout time of small tungsten filaments[6]. The oxygen contamination at fill time was less than 0.1 ppm, and remained at this

level for periods of weeks. No purification of the argon was found to be necessary and none was attempted.

3. Test Results

The modules were tested at SLAC in an e^- beam from .125 to 4 GeV/c and a π^- beam from 1 to 4 GeV/c. For tests at 1 GeV/c and above, π's and e's were selected by changes in the target and production angle, by the introduction of lead at the first focus of the beam, and with the use of two Freon 13 filled threshold Cerenkov counters placed upstream of the dewar. Each of the Cerenkov counters was measured to be more than 99% efficient on electrons. The momentum spread of the beam, 1.8% (FWHM) above 1 GeV/c, increasing to 3% at .125 GeV/c, was negligible.

The modules were large enough to contain electromagnetic showers in the radial direction at all relevant energies and to have 97% containment in the longitudinal direction at 4 GeV/c. This resulted in a response which was linear at low energies, with a slight deviation only at the highest energy point, as shown in Figure 3. The curve is a linear fit to the data up to 2 GeV/c. The energy loss of non-interacting π^- is also shown. No significant change in energy loss for pions is observed between 1 and 4 GeV/c.

While we were most concerned with the energy resolution of the detectors for photon initiated showers, it is most practical to test them in an electron beam. The energy resolution for low energy electrons is substantially degraded by energy loss in material in front of of the detector. We studied this effect by placing aluminum blocks in the beam just upstream of the detector. For the tests of module B, in

addition to the 0.1 r.l. of the dewar entrance window, the electrons traversed about 0.1 r.l. in beam defining scintillation counters and 0.25 r.l. in the two Cerenkov counters. For the tests of module A below 1 GeV/c, the Cerenkov counters were removed. In order to obtain the inherent energy resolution of the devices, the measurements with additional Al in the beam were used to extrapolate to zero material before the detector. In addition, an electromagnetic shower Monte Carlo calculation was used to verify the extrapolation.

Figure 4 shows the measured resolution of module B for electrons of several momenta, with and without additional aluminum placed in the beam. The degradation in resolution due to energy loss before the detector is clearly more pronounced at lower energies. The measurements were used to extrapolate to the expected resolution for photons. For module A below 1 GeV/c, the corresponding corrections were smaller.

Figure 5a shows the measured resolution for module A as a function of electron momentum. The dashed curve is the result of a Monte Carlo shower calculation of the energy deposited in the argon of a detector with alternate layers of lead and liquid argon preceded by .25 r.l. of Al. The solid curve is the sum in quadrature of the shower calculation and the total of 12 MeV of measured r.m.s. electronic noise. Figure 5b shows the resolution of module A extrapolated to zero material upstream of the counter. The curve is again the sum in quadrature of the Monte Carlo calculation, this time with no extra material in the beam, and the measured electronic noise. The fluctuations in the shower calculation are well represented by $6.5\%/\sqrt{E_e(\text{GeV})}$. Figure 5c shows the

resolution of module B extrapolated to zero additional material in the beam. The curve is the sum in quadrature of the Monte Carlo calculation, which is well represented by $9.5\%/\sqrt{E_e(\text{GeV})}$ and 12 MeV of electronic noise. The resolution of the two modules is consistent with $t^{-\frac{1}{2}}$ as expected from the calculations shown in Figure 1.

The energy response curves of module A at several electron monenta are shown in Figure 6 together with curves representing the best least squares fit of a gaussian. These represent the data well, with the exception of small low energy tails due to energy loss upstream.

It is possible to improve the low energy resolution of the device somewhat by using only the front part of the module, so as not to add unnecessary electronic noise. This is illustrated in Figure 7, where the resolution is shown as a function of the depth of the device utilized. It is seen that the test module is well matched to 1 GeV, but could have better resolution at high energy if fluctuations due to energy loss out the back were reduced. More importantly, the resolution at low energy can be improved by ignoring the last 4.5 r.l. of the module. This has not been done in the resolution vs. energy curves of Figure 5.

The longitudinal distribution of shower energy could be sampled in groups ending at 2.25,4.5,6.75,10.25 and 15.75 r.l. These distributions are shown for incident momenta of .25, 1 and 4 GeV/c in Figure 8. The expected logarithmic increase of shower maximum with energy is clearly evident. These curves make it clear that a shower detector intended for use below several GeV must incorporate electronics with a

wide dynamic range. This problem is further accentuated by the large fluctuations about the mean energy deposited at a given depth. Figure 9 shows the actual distribution of energy in each of the five depths at incident electron momenta of .25 GeV/c and 4 GeV/c. The curves at the two energies are normalized to 100% of the charge deposited at each energy separately, so that the 4 GeV/c scale is sixteen times that of the .25 GeV/c scale. It will be seen that the fluctuations of the .25 GeV/c curves are very large, such that it is not improbable that only a small amount of energy will be deposited after 4.5 r.l. Aside from the requirements this places on the dynamic range of a channel at a given depth, it is clear that a detector which is to be used to measure the position of the shower in this energy range must determine both coordinates and resolve ambiguities very early in the shower, typically in the first three or four radiation lengths. This is easily accomplished by interleaving different coordinate strips at the front of the module.

The data in Figures 3-9 were obtained with the high voltage set to 3 kV, or a field of 15 kV/cm. The operating plateau is very wide; signals can be seen at 250 volts. The collected charge and resolution for a 1 GeV/c e^- as a function of electric field for module A are shown in Figure 10.

Since some of the shower counter modules for the Mark II Detector will be placed in a transverse magnetic field of a few hundred gauss and in longitudinal fields of up to 5 kG, a test of the effect of a magnetic field on the charge collected and on the resolution of the module was made.

Calculations indicate that the device is not likely to be affected by reasonable fields, but the region of onset of measurable effects is sensitive to assumptions about the distribution of low energy shower tracks. Data were therefore taken for .25 GeV/c and 1 GeV/c electrons in a transverse magnetic field of up to 1.3 kG. The results at 1 GeV/c are shown in Figure 11. No significant effect was seen at either energy at any field.

The 2 cm. wide collection strips were grouped such that we obtained three samples of the transverse shower spread for each of the five depths. All of the strips were parallel; the shower distribution is projected onto a single transverse coordinate (x-axis). Since the electron beam size was larger than the expected spatial resolution, we measured the resolution on an event-by-event basis. Two methods were employed.

In the simpler method, the centroid and variance for the shower were computed in each of the five layers. A least squares fit of a straight line was then made to these five centroids, and the residuals in each layer were then found. The r.m.s. deviations are plotted for 1 GeV/c electrons in Figure 12. It is seen that a spatial resolution of a few millimeters is achieved with the present 2 cm. strip width. Figure 13 shows the actual distribution of the residuals in the first two radiation lengths for a 1 GeV/c electron.

The second method involved a fit to the pulse height distribution at each depth. For convenience, we assume a Gaussian shape and fit for the mean and width (x_i, σ_i) at each depth. A preliminary fit is made

for each depth and the resulting five means (x_i) are then fit to a straight line representing the electron direction. The Gaussian widths are then re-fit with the means constrained to the values given by the straight line fit. The results for this constrained fit are shown in Figure 14. The transverse width of the shower is independent of the electron energy over the region studied, although the fluctuations are of course larger at low energies.

The spatial resolution is given by the error in the mean for the Gaussian fit. To calculate this error, we must estimate the number of independent tracks at each depth in the shower. To obtain the estimate, we divide the total pulse height for each cell by the pulse height corresponding to a single minimum ionizing particle. The fit is then made with a maximum likelihood technique using Poisson statistics on the estimated number of independent tracks. The spatial resolution results for the uncorrelated error in the mean (Δx_i) are shown in Figure 15. We have made an independent check on our estimate of the errors by studying the χ^2 distribution for the straight line for the means. The χ^2 distributions show more events at smaller χ^2 than one would expect for three degrees of freedom indicating that our errors are slightly over-estimated or that correlations exist from depth to depth.

One of the most important functions of an electromagnetic shower detector is the separation of hadrons from electrons, and in particular, the identification of electrons in a large background of pions. The ratio of absorption length to radiation length is large for a lead-liquid argon detector, (typically 25-30) and the counter is easily subdivided longitudinally and radially to measure the different characteristics of

hadronic and electromagnetic showers. Results on proton/electron separation have been recently reported by Engler, et al.[7], for a detector similar to those discussed here.

Our tests involved π^- and e^- at 1,2 and 4 GeV/c, with and without 1 r.l. of Al in front of the device to simulate the effects of a solenoid coil. Although it is possible to use maximum likelihood techniques to effect the π^-/e^- separation, we have confined ourselves here to a series of simple orthogonal cuts on total energy deposition, and on the longitudinal and radial deposition of shower energy. At energies above 1 GeV/c the primary means of e^-/π^- discrimination is comparison of the total energy deposition in the device. This is shown for 2 GeV/c e^- and π^- in Figure 16. Study of the energy division between the front and back of the detector can improve the separation markedly, however, especially at low energies. The distribution of charge in the first two radiation lengths ($Q_{1,2}$) vs. the total (Q_{tot}) was studied, as was the distribution of charge in the first four radiation lengths (Q_{1-4}) vs. the total. There is also a difference between the radial spread of hadronic and electromagnetic showers, which can be used to gain a slight improvement in π/e separation, although a drastic improvement in separation can only be achieved at the expense of electron efficiency. Figure 17 shows a scatterplot of the energy deposited in the first two radiation lengths versus the r.m.s. deviation of the distribution of charge among three of the 2 cm. strips ($\sigma^2 = \Sigma\, Q_i\, (x - \bar{x})^2 / \Sigma\, Q_i$), for 4 GeV/c π^- and e^-. It will be seen that those π^- with large $Q_{1,2}$, i.e., those which interact in or before the first two radiation lengths tend to have a larger σ. Thus a cut on the maximum variance

can remove some π^-, but a cut which removes a large number of π^- necessarily sharply reduces electron efficiency. Our devices measured only a single projection of the shower; cuts on both transverse projections would improve the π/e rejection somewhat. In Figures 18,19 we show scatterplots of $Q_{1,2}$ vs. Q_{tot} and Q_{1-4} vs. Q_{tot}. This data has already been cut on maximum $\sigma_{1,2}$ or σ_{1-4}. Clearly, most of the π/e rejection comes from the differences in Q_{tot} but substantial improvement in rejection can be achieved by also using the differences in energy deposition in the front of the detector. Figure 20 summarizes the power of these cuts for data with and without 1 r.l. of aluminum before the detector. Since π^- charge exchange amounts to ~1% in 1 r.l. of Al at these energies, the π^-/e^- rejection ratio does suffer somewhat with the additional material. Without the Al, it is possible to achieve a π^- efficiency as low as 7×10^{-3} with 90% electron efficiency at 1 GeV/c. At higher energies substantially better separation can be achieved.

4. Conclusion

Measurements of the energy resolution, spatial resolution, hadron/electron separation capability and other characteristics of a lead-liquid argon electromagnetic shower counter have been presented. The performance of the device has encouraged us to adopt this technique for shower detection in the Mark II Detector Facility at SPEAR.

We wish to thank W. J. Willis, J. Lindsey, V. Radeka and other members of the IMP Group for helpful conversations, R. Gearhart for his efforts in establishing the low energy beams required for these tests, and D. Hunt and R. Fuzesy for the design and construction of the cryogenic system.

REFERENCES

1. W. J. Willis and V. Radeka, Nucl. Instr. and Meth. 120, 221 (1974).
2. J. Engler, B. Friend, W. Hofmann, H. Keim, R. Nickson, W. Schmidt-Parzefall, A. Segar, M. Tyrrell, D. Wegener, T. Willard and K. Winter, Nucl. Instr. and Meth. 120, 157 (1974).
3. G. Knies and D. Neuffer, Nucl. Instr. and Meth. 120, 1 (1974).
4. B. Rossi, High Energy Particles (New York, Prentice Hall, 1952).
5. Thanks are due to W. J. Willis, J. Lindsey and V. Radeka for their aid in duplicating their preamp and shaping amplifier circuitry.
6. Designed by E. Hoyt and W. P. Schulz, SLAC Physical Electronics Grp.
7. J. Engler, W. Hofmann, J. Spengler and D. Wegener, Karlsruhe preprint, 1976.

FIGURE CAPTIONS

1. Dependence of resolution on plate thickness for 1 GeV/c electrons in a sampling detector with lead plates. Curve a shows the $t^{-\frac{1}{2}}$ dependence expected from analytic shower theory. Curve b is the result of a Monte Carlo shower calculation. σ is the r.m.s. deviation of the ionization energy deposited in 2 mm. gaps of liquid argon. The total depth of the device was held constant at 16 radiation lengths.
2. Grouping of channels in width and depth in the test modules. All groups consisted of 2 cm. wide strips running in the vertical direction only.
3. Collected charge in minions (1 minion = charge collected for the passage of a minimum ionizing particle through a minimum grouping of cells, i.e., through six gaps) vs. momentum of incident e^- and (non-interacting) π^-.
4. Energy resolution of module B for electron momenta from .25 to 4 GeV/c as a function of the amount of aluminum placed upstream of the detector.
5. a) Measured resolution of module A as a function of electron momentum. The dashed curve is a Monte Carlo shower prediction with .25 r.l. of aluminum upstream of the detector. The solid curve is the sum in quadrature of the shower calculation and 12 MeV of r.m.s. equivalent electronic noise. b) Resolution of module A extrapolated to zero material upstream of the counter. The error in the resolution at low energies is principally due to the

extrapolation to zero beam material. The curve is the sum in quadrature of the shower calculation (with no extra material) and the electronic noise. c) Resolution of module B extrapolated to zero material upstream of the counter. The curve is the sum in quadrature of the shower calculation (with no extra material) and the electronic noise.

6. Pulse height distributions in module A for a) 0.25, b) 1.0 and c) 4.0 GeV/c electrons.
7. Resolution (σ/E) vs. effective depth of the shower counter. Note that the resolution at lower energies can be improved by using only the first twelve radiation lengths, since the electronic noise contribution outweighs the signal at this depth in a low energy shower.
8. Deposition of collected shower energy in five sampling depths for 0.25, 1.0 and 4.0 GeV/c electrons.
9. Distribution of shower energy within the five sampling depths for a) 0.25 and b) 4 GeV/c electrons. The abscissa at each momentum is the fraction of the mean total energy observed. Thus, the 0.25 and 4 GeV/c scales differ by a factor of 16.
10. a) Collected charge as a function of electric field for 1 GeV/c electrons. b) Resolution (σ/E) in percent as a function of electric field for 1 GeV/c electrons. The curves are drawn to guide the eye.
11. a) Pulse height normalized to zero field vs. transverse magnetic field for 1 GeV/c electrons. b) R.m.s. deviation of the distribution of pulse height (normalized to zero field) vs. transverse magnetic field for 1 GeV/c electrons.

12. The r.m.s. deviations from the best fit straight line to the centroids of the charge deposition in different layers in depth for 1 GeV/c electron showers.
13. Distribution of the deviations from the best fit straight line in the first two radiation lengths for 1 GeV/c electrons.
14. Lateral shower spread in one dimension in each of the five depths for 1, 2 and 4 GeV/c electron showers.
15. Position uncertainty for 1 GeV/c electron showers as a function of strip width at different depths. The calculated curves are described in the text.
16. a) Total pulse height (Q_{tot}) in minions for 2 GeV/c electrons. b) Total pulse height (Q_{tot}) in minions for 2 GeV/c π^-.
17. Distribution of shower width vs. charge deposited in the first two radiation lengths for a) 4 GeV/c e^- and b) 4 GeV/c π^-.
18. Charge deposited in the first two radiation lengths vs. total charge for a) 1 GeV/c e^- and b) 1 GeV/c π^-. The distributions have been cut on the maximum width of the shower.
19. Charge deposited in the first four radiation lengths vs total charge for a) 1 GeV/C e^- and b) 1 GeV/c π^-. The distributions have been cut on the maximum width of the shower.
20. π^-/e^- rejection figures for 1,2 and 4 GeV/c particles with and without 1 r.l. of aluminum placed in front of the module. Curves are plotted for cuts on the charge in the first two r.l. ($Q_{1,2}$) vs. Q_{tot} with an additional cut on the shower width at the front of the device.

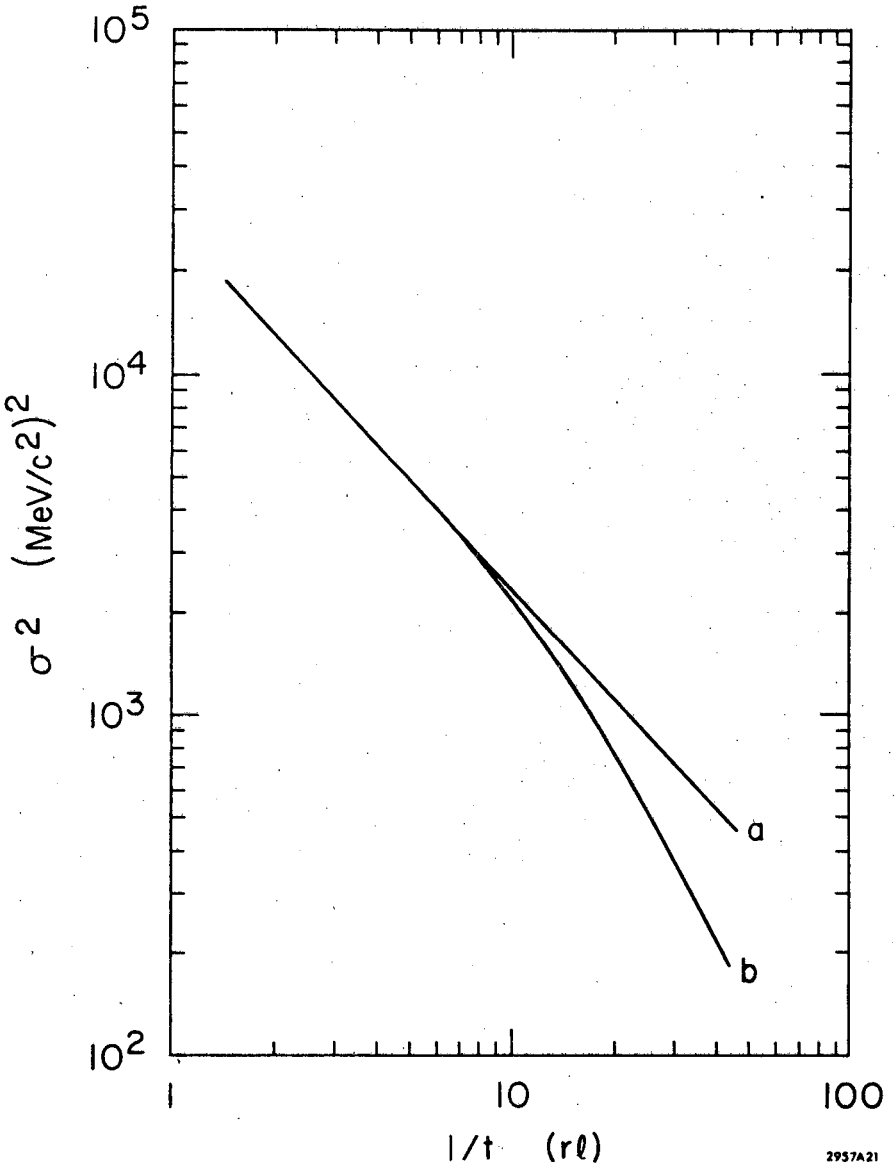
10^5
10^4
10^3
10^2
σ^2 (MeV/c^2)^2
a
b
1
10
100
1/t (rℓ)
2957A21

Fig. 1

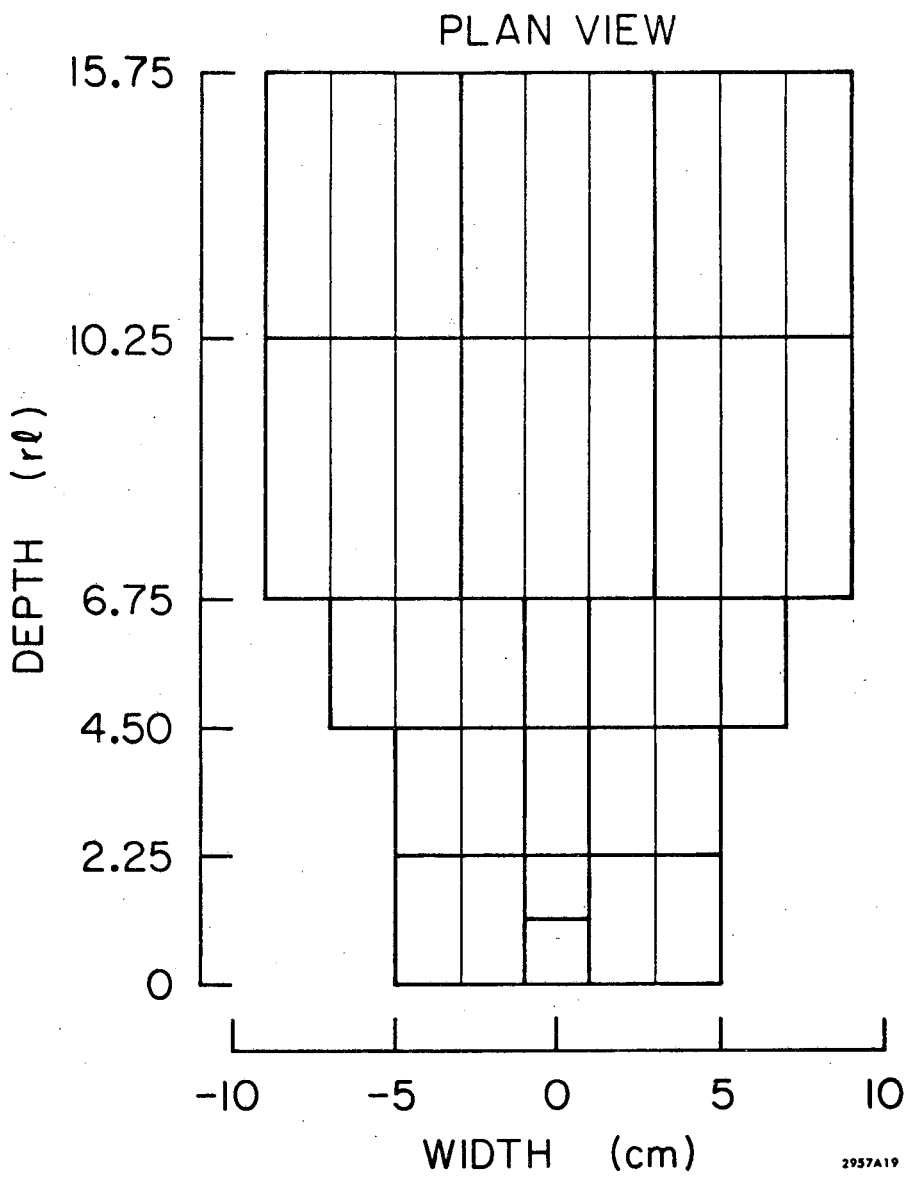
PLAN VIEW
15.75
10.25
6.75
4.50
2.25
0
DEPTH (rℓ)
-10
-5
0
5
10
WIDTH (cm)
2957A19

Fig. 2

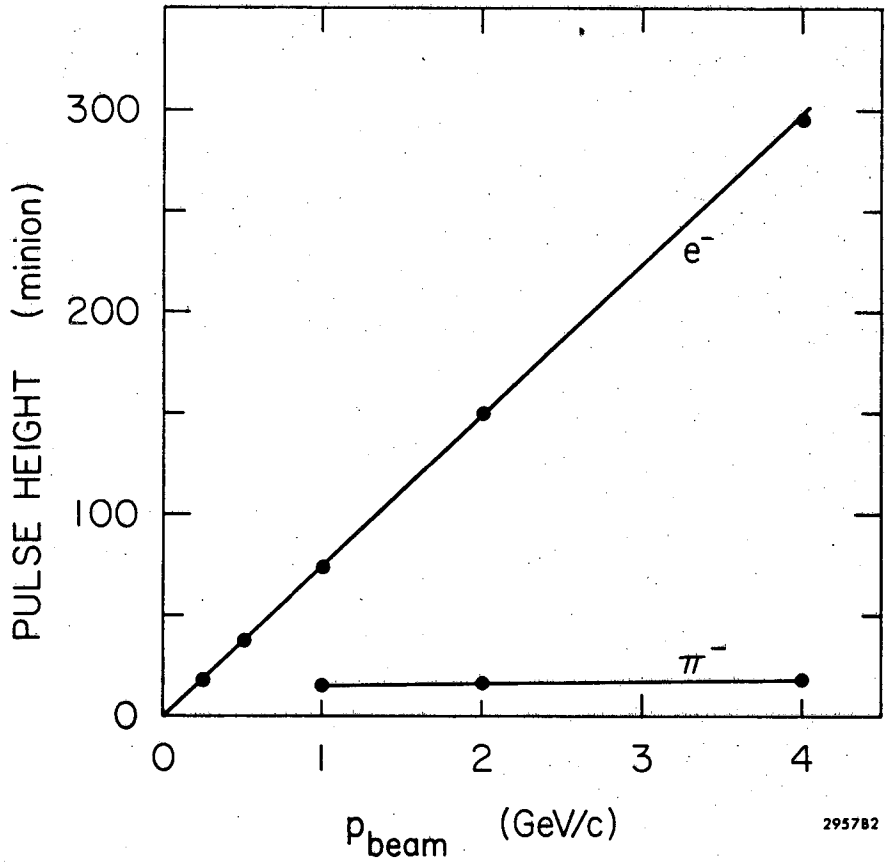
PULSE HEIGHT (minion)
300
200
100
0
0
1
2
3
4
p_{beam} (GeV/c)
e^-
π^-
295782

Fig. 3

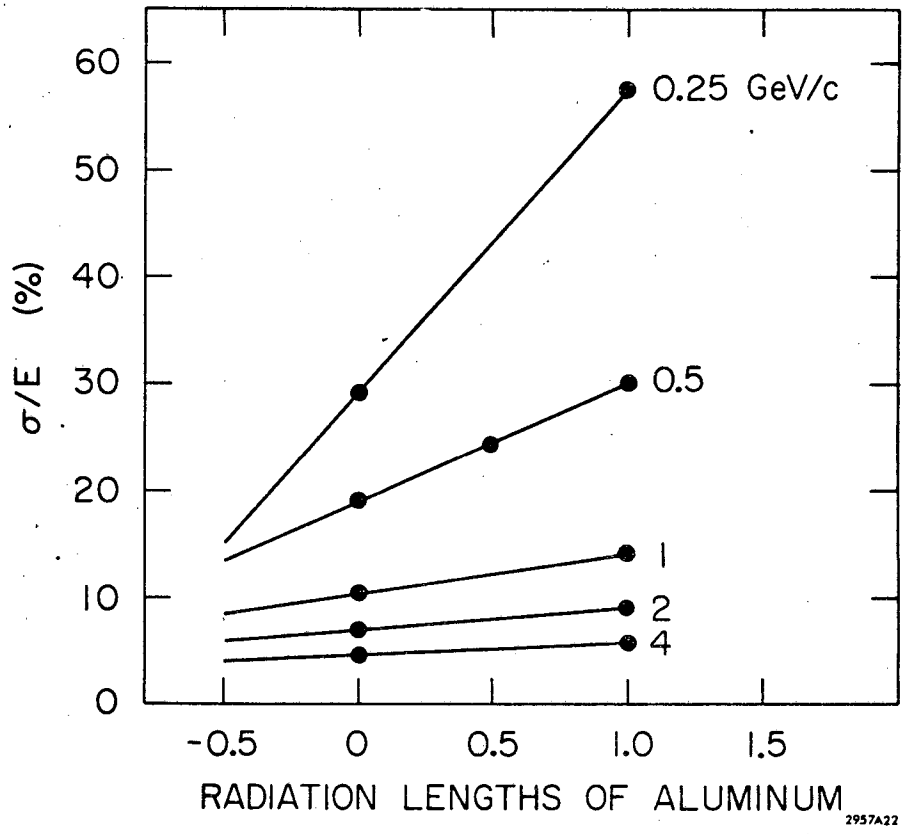
σ/E (%)
60
50
40
30
20
10
0
-0.5
0
0.5
1.0
1.5
RADIATION LENGTHS OF ALUMINUM
0.25 GeV/c
0.5
1
2
4
2957A22

Fig. 4

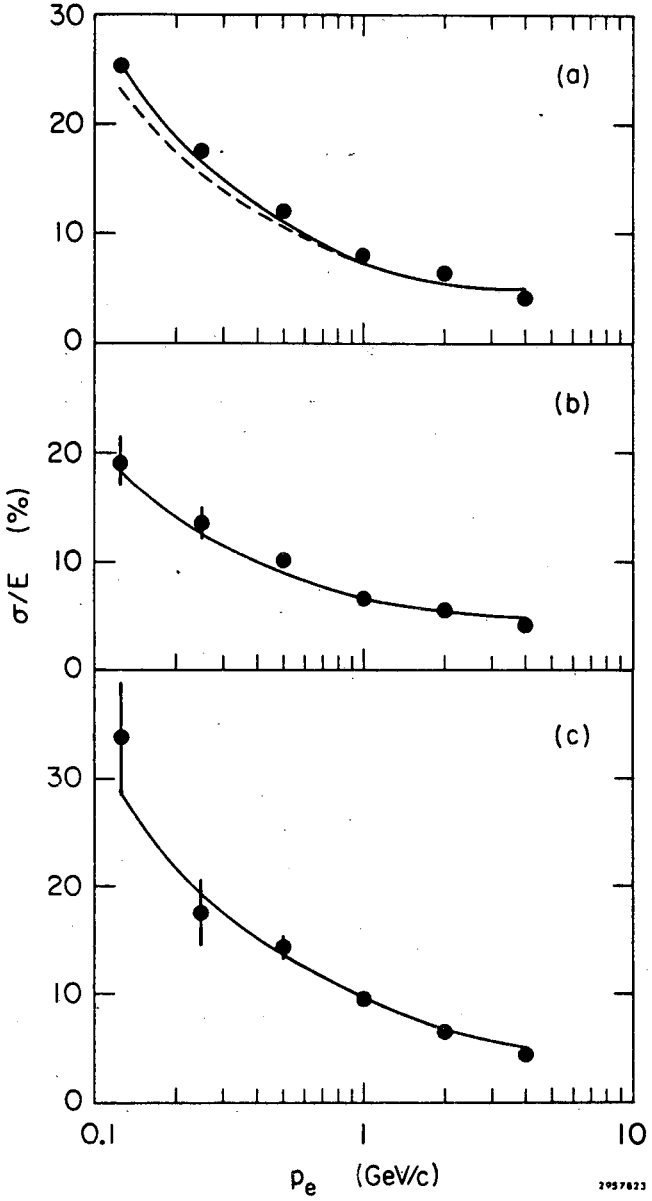
(a)
(b)
(c)
σ/E (%)
p_e (GeV/c)

Fig. 5

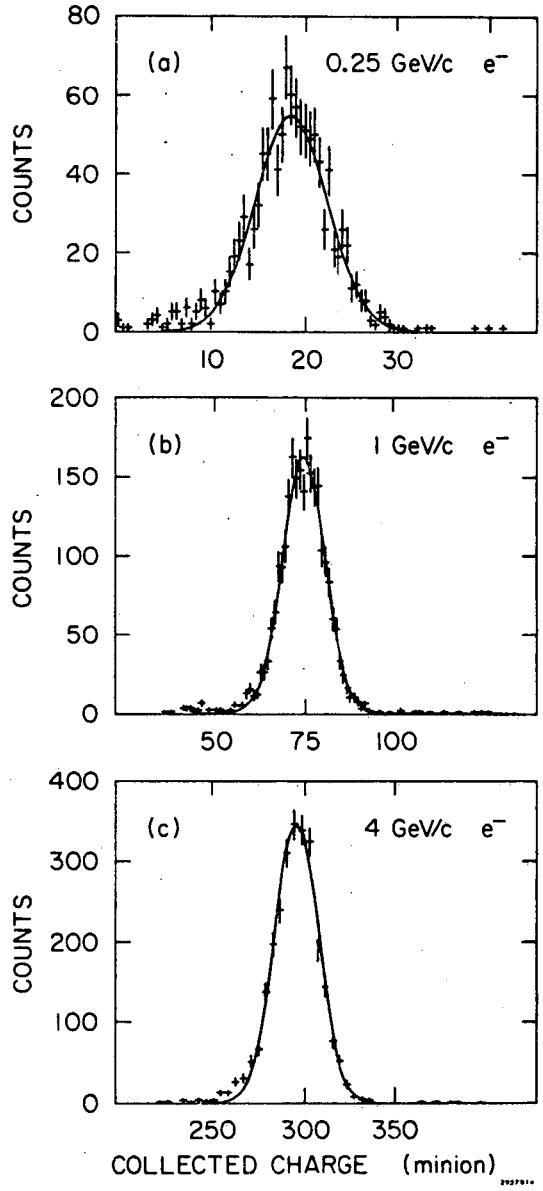
(a) 0.25 GeV/c e⁻
(b) 1 GeV/c e⁻
(c) 4 GeV/c e⁻
COUNTS
COLLECTED CHARGE (minion)

Fig. 6

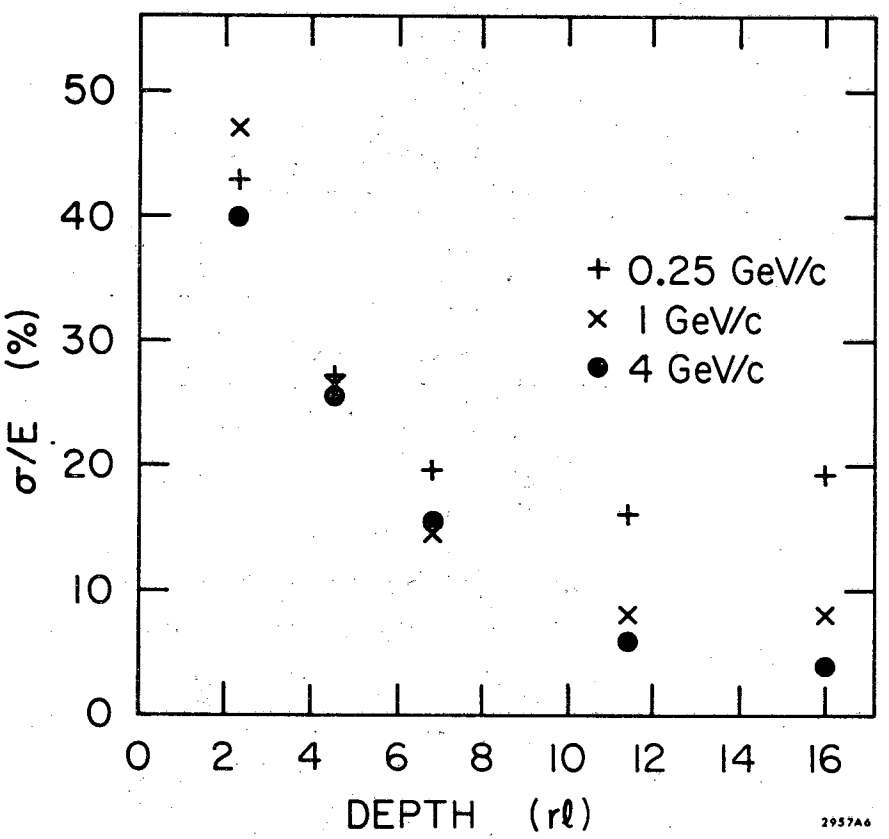
σ/E (%)
50
40
30
20
10
0
0 2 4 6 8 10 12 14 16
DEPTH (rℓ)
+ 0.25 GeV/c
× 1 GeV/c
● 4 GeV/c
2957A6

Fig. 7

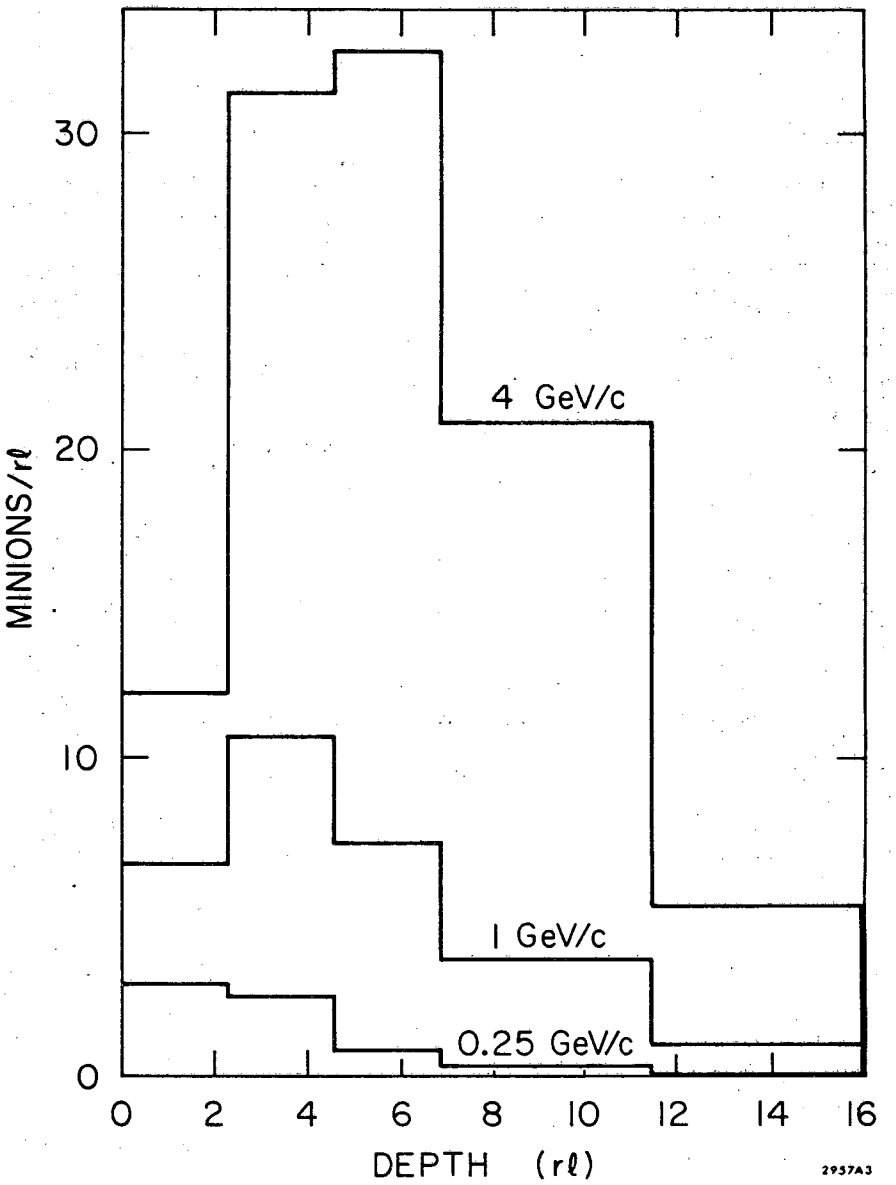
MINIONS/rℓ
30
20
10
0
0 2 4 6 8 10 12 14 16
DEPTH (rℓ)
4 GeV/c
1 GeV/c
0.25 GeV/c
2957A3

Fig. 8

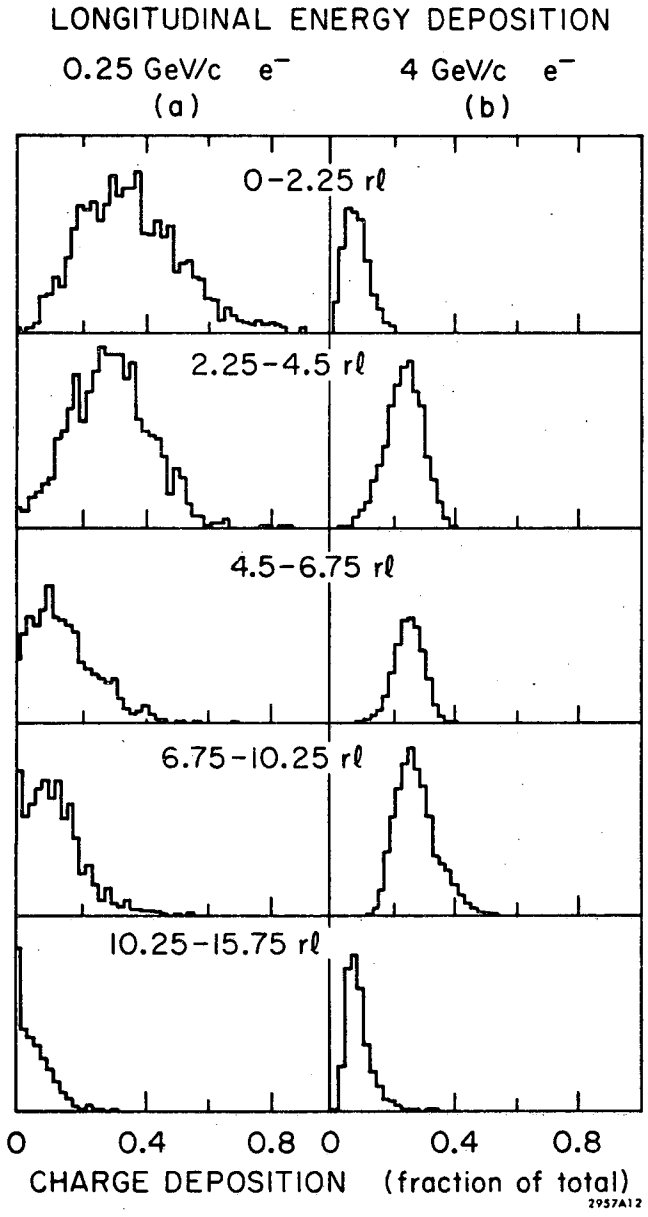
LONGITUDINAL ENERGY DEPOSITION
0.25 GeV/c e⁻
(a)
4 GeV/c e⁻
(b)
0-2.25 rℓ
2.25-4.5 rℓ
4.5-6.75 rℓ
6.75-10.25 rℓ
10.25-15.75 rℓ
0
0.4
0.8
0
0.4
0.8
CHARGE DEPOSITION (fraction of total)
2957A12

Fig. 9

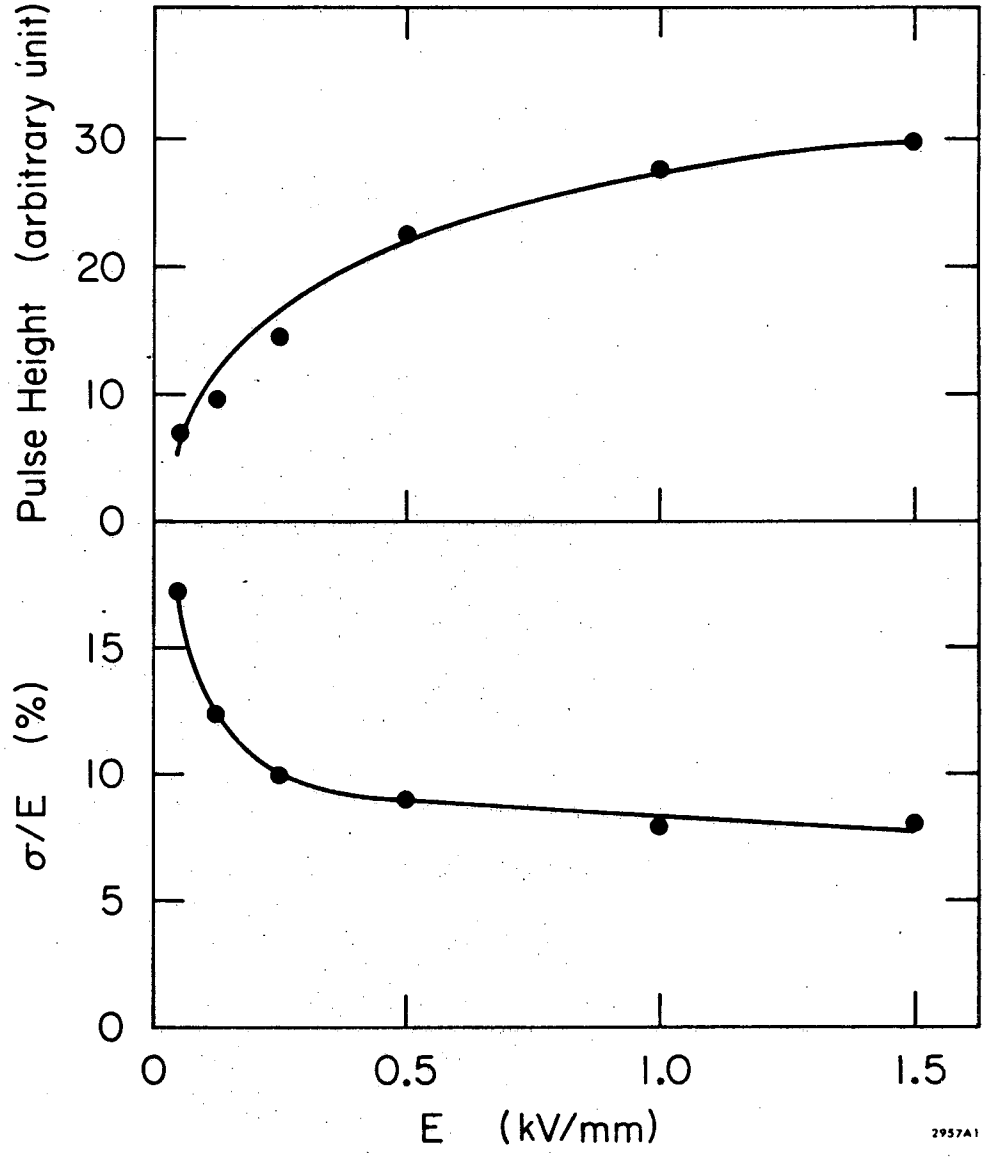
Pulse Height (arbitrary unit)
30
20
10
0
σ/E (%)
15
10
5
0
0
0.5
1.0
1.5
E (kV/mm)
2957A1

Fig. 10

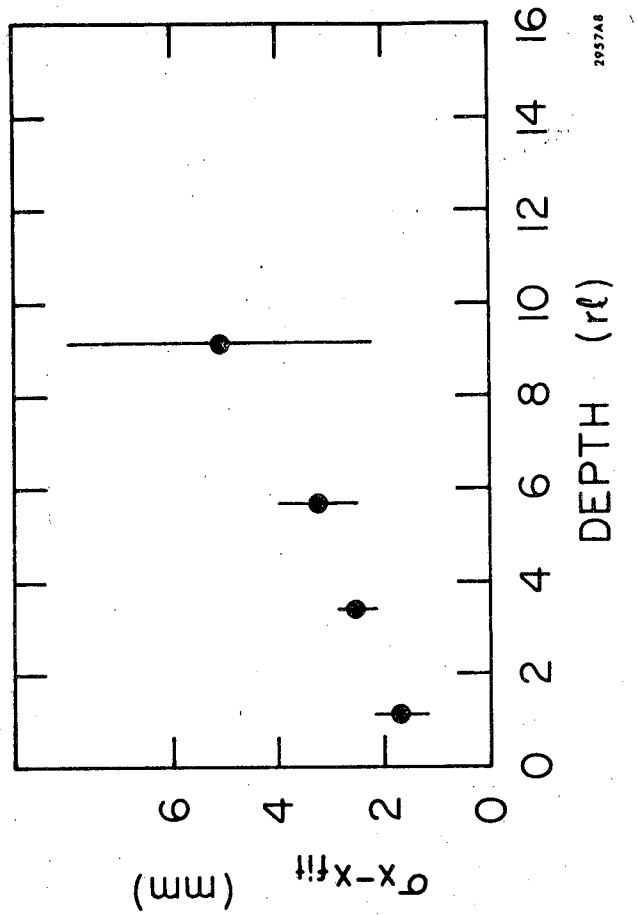
$\sigma_{x-x_{fit}}$ (mm)
0
2
4
6
8
0
2
4
6
8
10
12
14
16
DEPTH (rℓ)
2937A18

Fig. 12

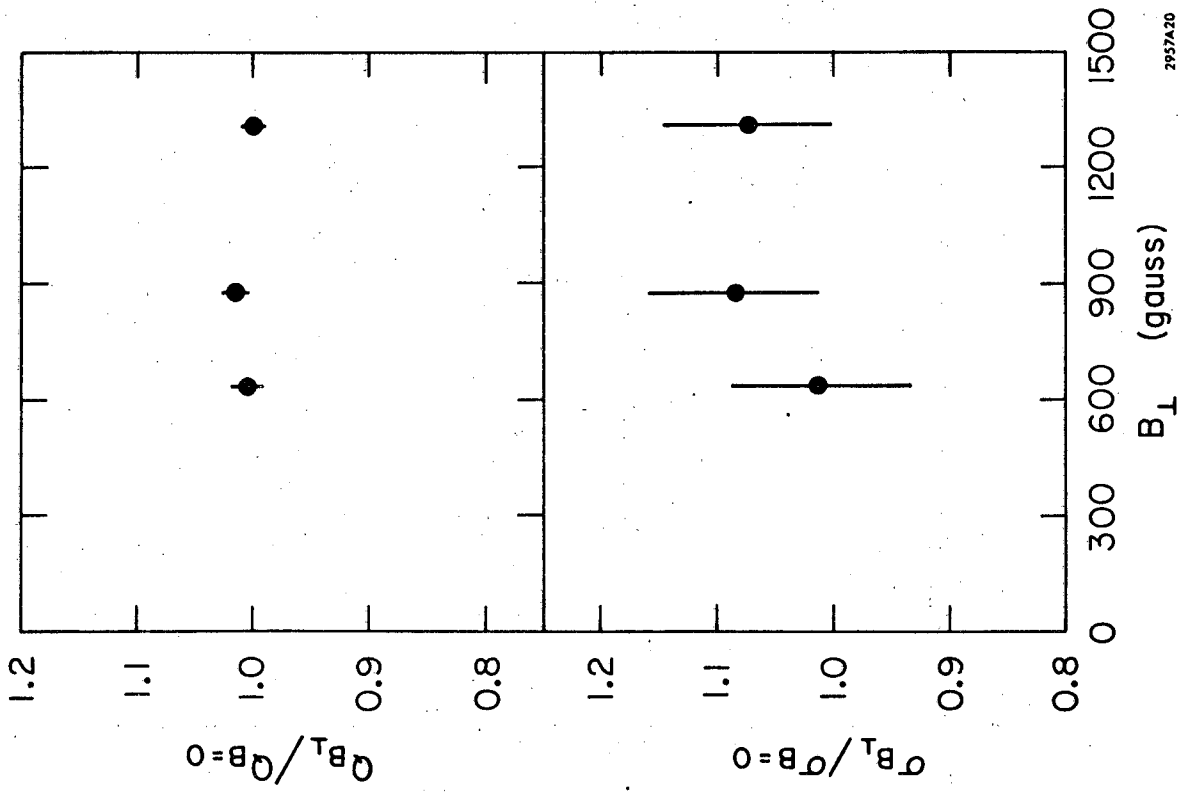
$Q_{B_\perp}/Q_{B=0}$
$\sigma_{B_\perp}/\sigma_{B=0}$
1.2
1.1
1.0
0.9
0.8
0
300
600
900
1200
1500
$B_\perp$ (gauss)
2957A20

Fig. 11

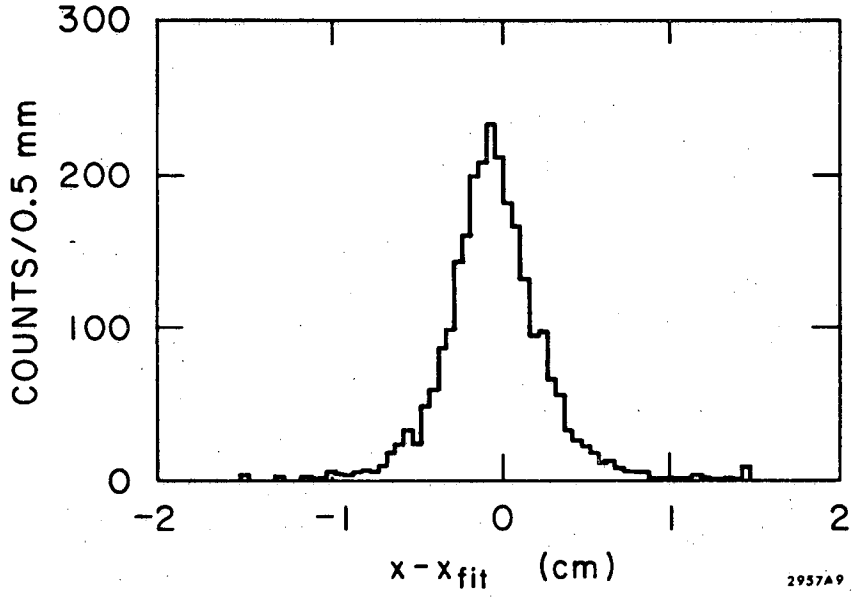
300
200
100
0
COUNTS/0.5 mm
-2
-1
0
1
2
x - x fit (cm)
2957A9

Fig. 13

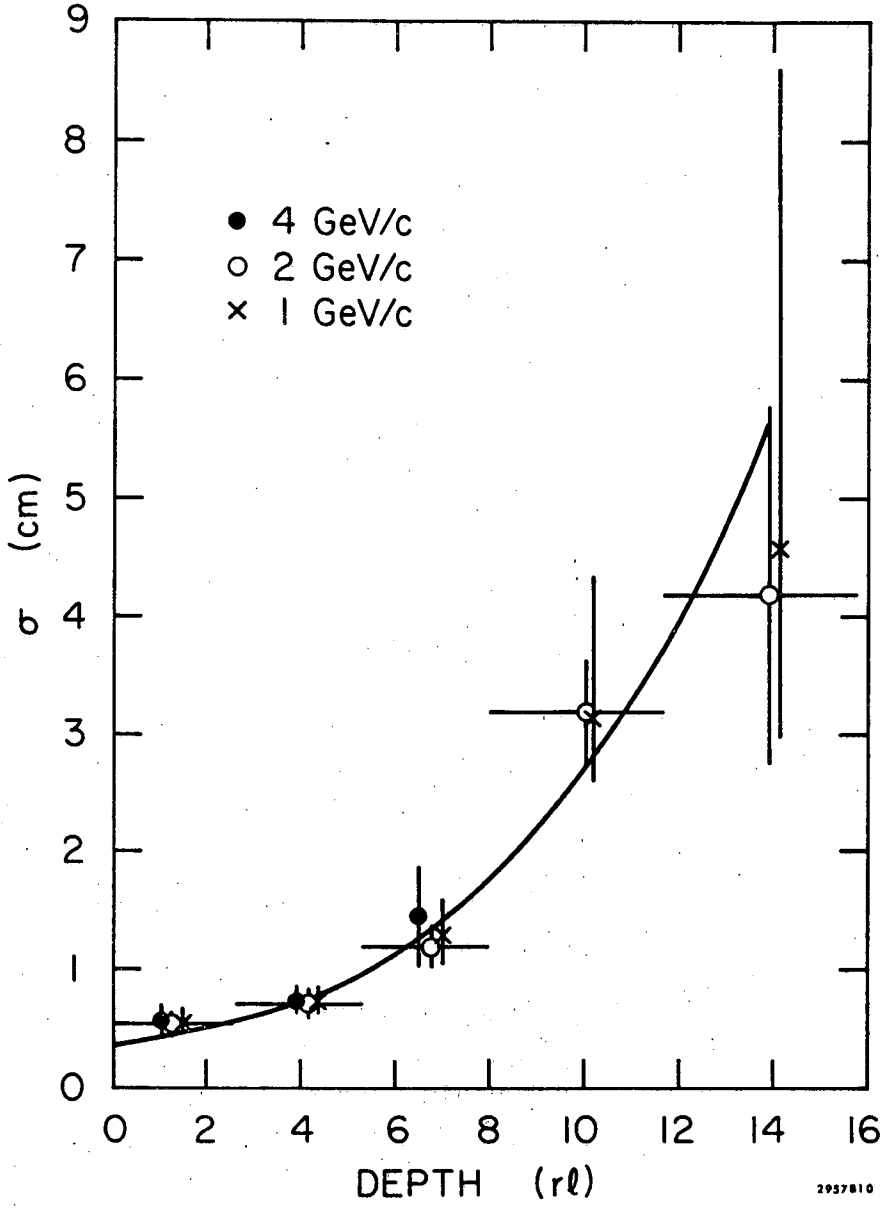
9
8
7
6
5
4
3
2
1
0
σ (cm)
● 4 GeV/c
○ 2 GeV/c
× 1 GeV/c
0
2
4
6
8
10
12
14
16
DEPTH (rℓ)
2957B10

Fig. 14

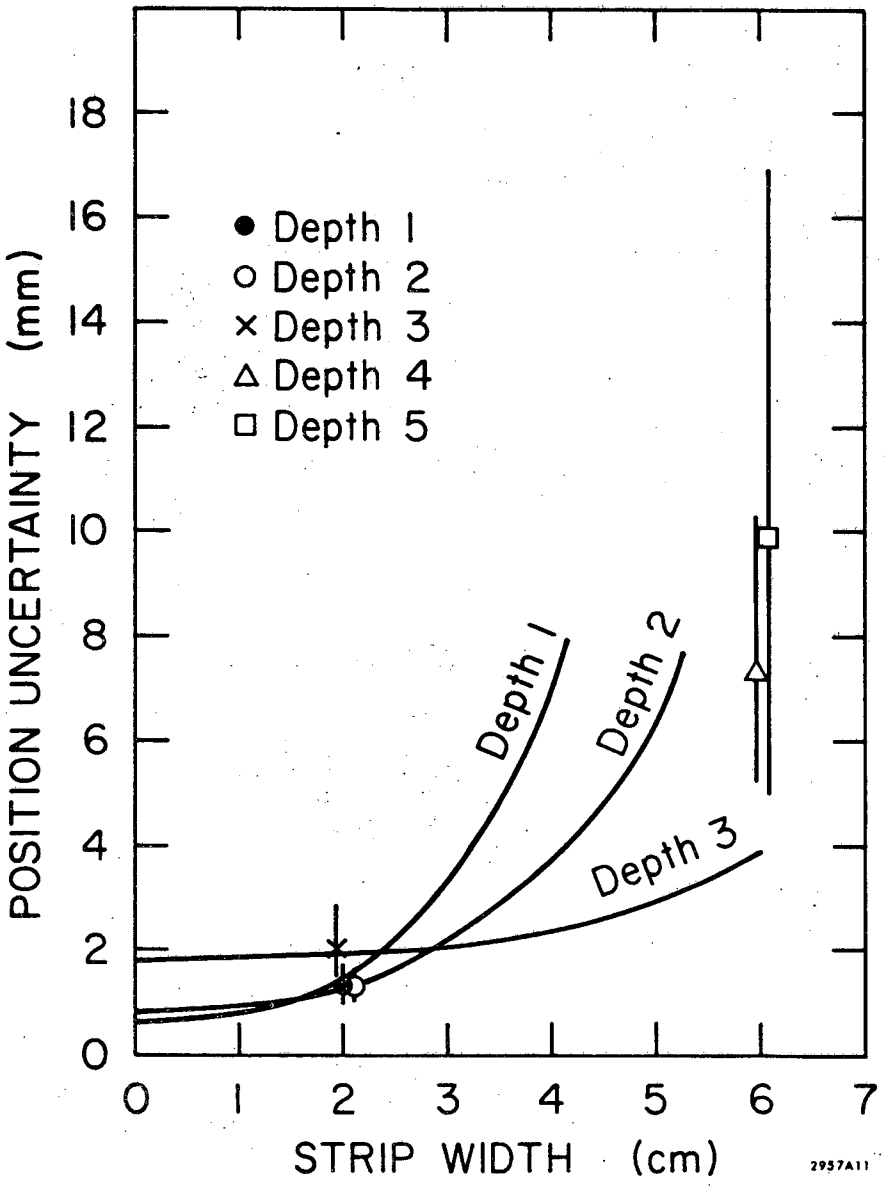
POSITION UNCERTAINTY (mm)
STRIP WIDTH (cm)
Depth 1
Depth 2
Depth 3
Depth 4
Depth 5
Depth 1
Depth 2
Depth 3
0
2
4
6
8
10
12
14
16
18
0
1
2
3
4
5
6
7
2957A11

Fig. 15

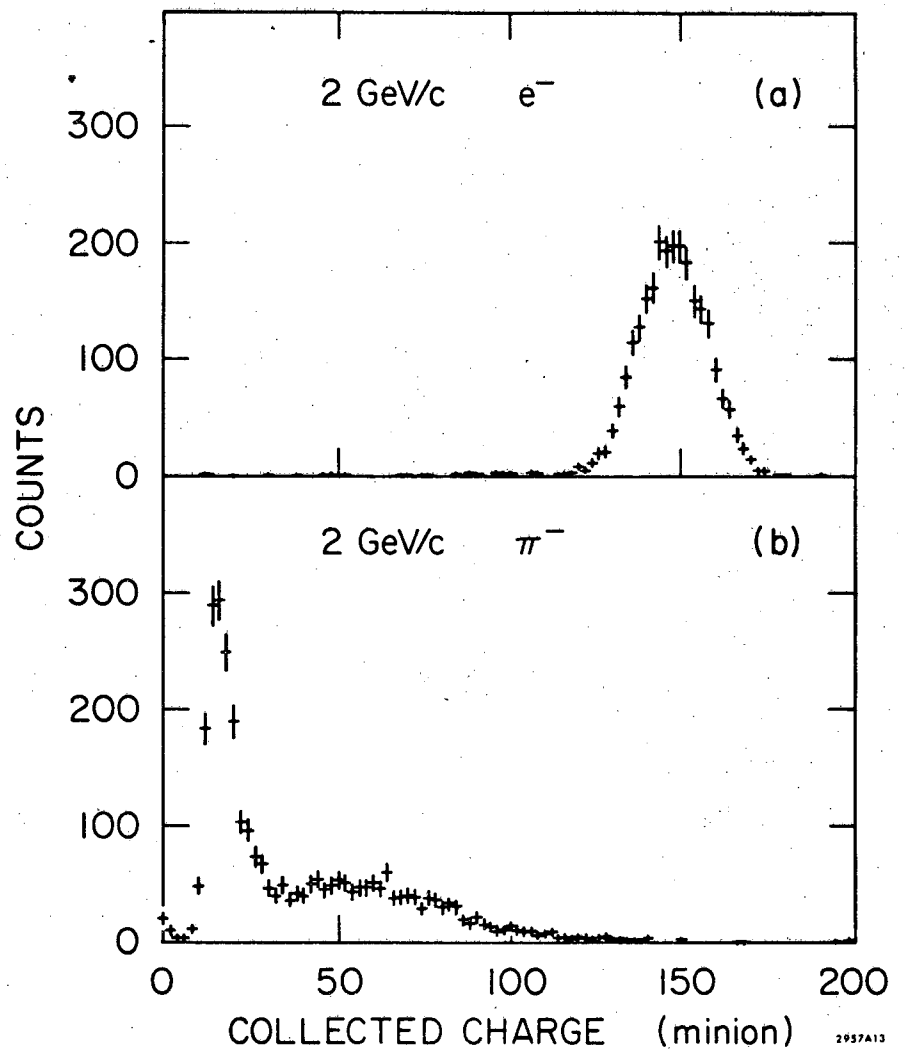
2 GeV/c e⁻
(a)
2 GeV/c π⁻
(b)
COUNTS
COLLECTED CHARGE (minion)
0
100
200
300
0
50
100
150
200
2957A13

Fig. 16

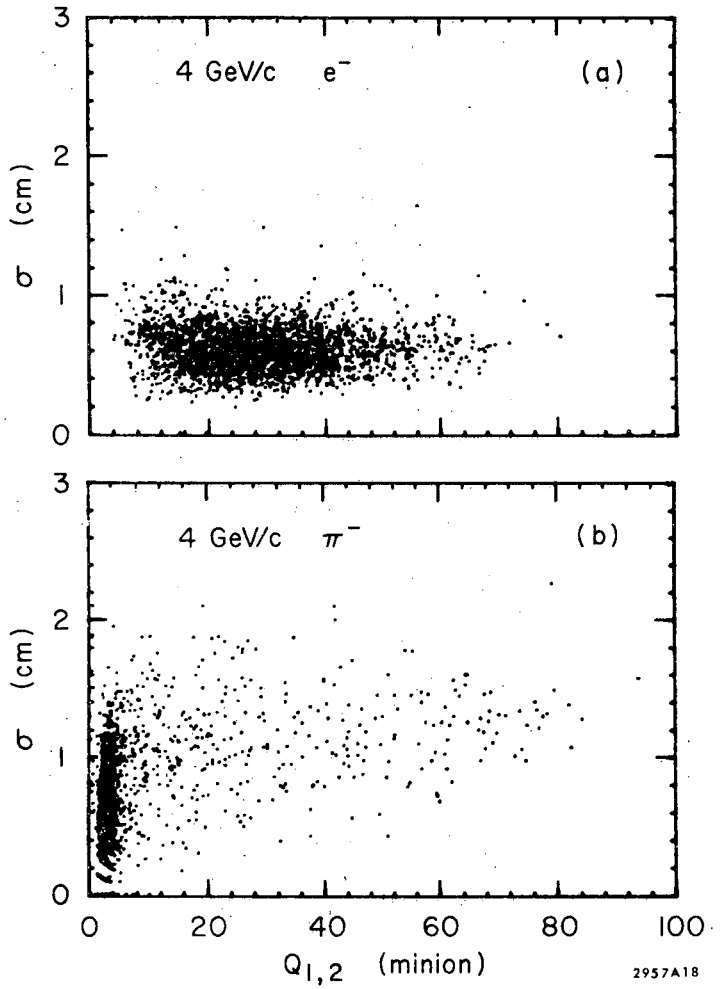
4 GeV/c e⁻
(a)
4 GeV/c π⁻
(b)
σ (cm)
Q1,2 (minion)
2957A18

Fig. 17

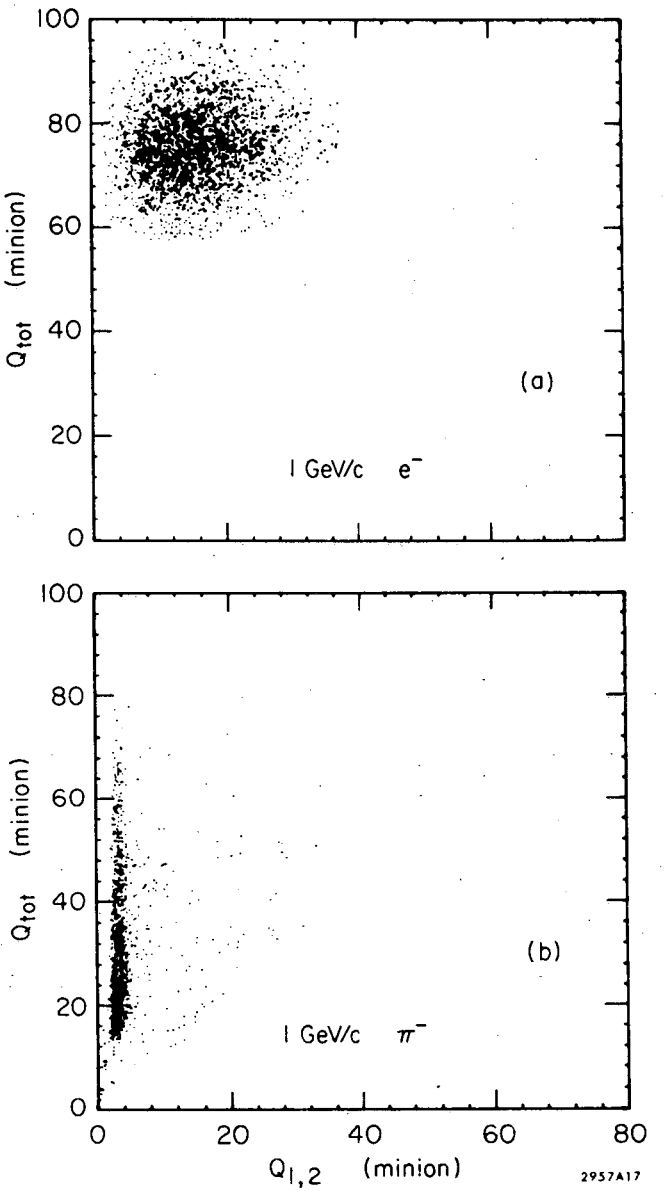
1 GeV/c e⁻
(a)
1 GeV/c π⁻
(b)
Qtot (minion)
Q1,2 (minion)
2957A17

Fig. 18

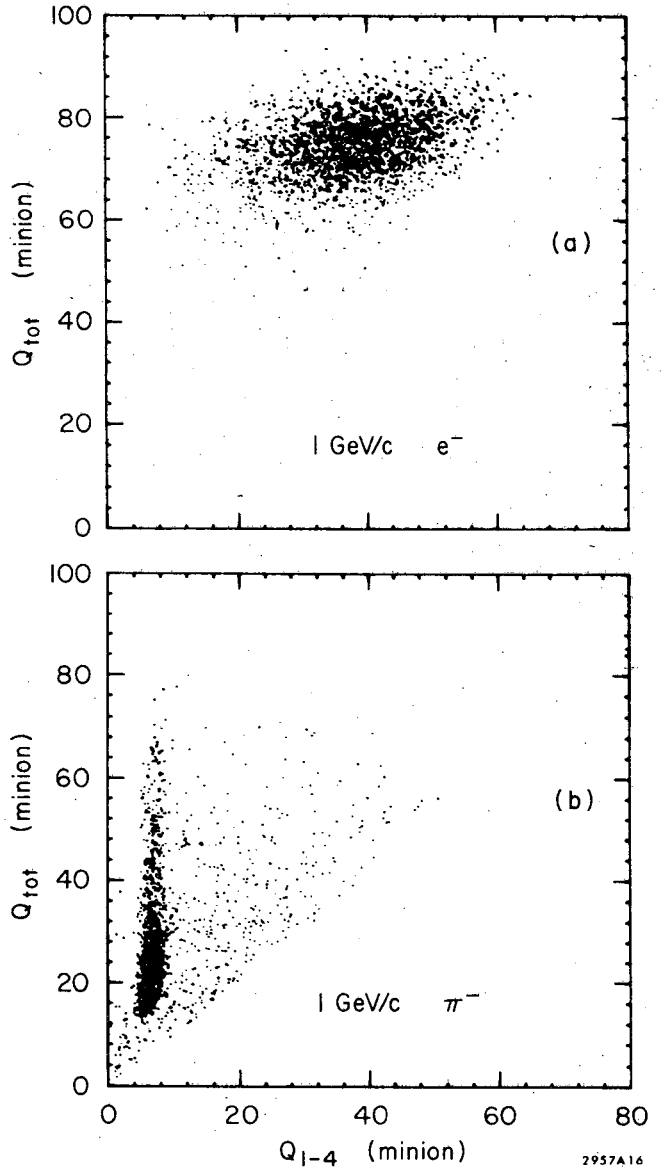
100
80
60
40
20
0
Q_{tot} (minion)
(a)
1 GeV/c e⁻
100
80
60
40
20
0
Q_{tot} (minion)
(b)
1 GeV/c π⁻
0
20
40
60
80
Q_{1-4} (minion)
2957A16

Fig. 19

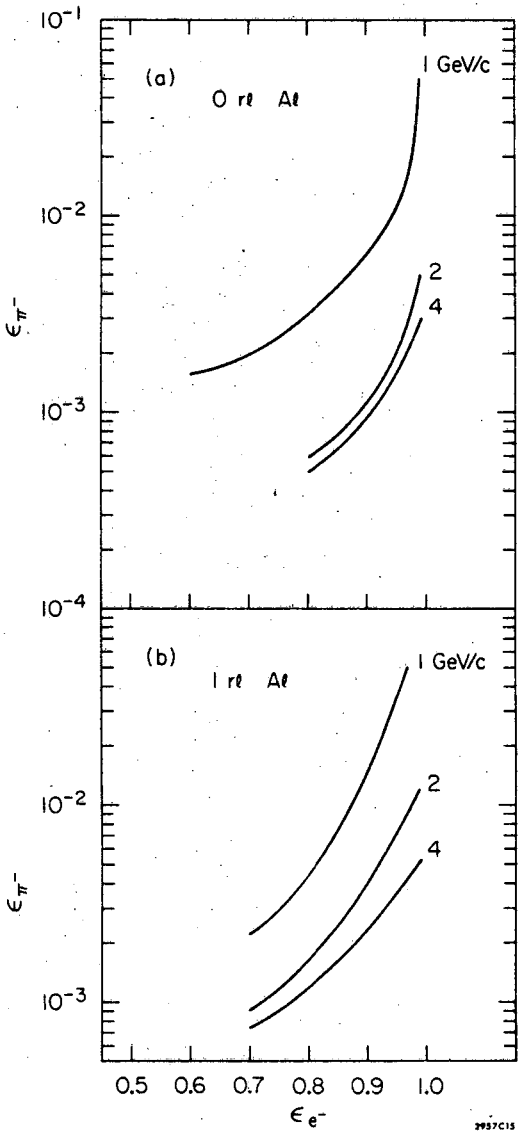
10^{-1}
10^{-2}
10^{-3}
10^{-4}
ϵ_{π^-}
(a)
O rℓ Aℓ
1 GeV/c
2
4
(b)
1 rℓ Aℓ
1 GeV/c
2
4
0.5
0.6
0.7
0.8
0.9
1.0
ϵ_{e^-}
2957C15

Fig. 20